http://dx.doi.org/10.5012/bkcs.2012.33.3.862

Calculation of the Absolute Rate of Human Cu/Zn Superoxide Dismutases from Atomic-Level Molecular Dynamics Simulations†

Jinuk Lee,‡ Woojin Lee,‡ Hwangseo Park,§ and Sangyoub Lee*

*Department of Chemistry, Seoul National University, Seoul 151-742, Korea. *E-mail: sangyoub@snu.ac.kr*
‡Corporate R&D Institute, Samsung Electro-Mechanics Co. Ltd., Suwon 443-743, Korea
§Department of Bioscience and Technology, Sejong University, Seoul 143-747, Korea
Received December 5, 2011, Accepted January 6, 2012

Based on the recently derived general expression for the rates of diffusion-controlled reactions, we calculate the rates of dismutation of the superoxide anion radical catalyzed by Cu/Zn superoxide dismutases (SOD). This is the first attempt to calculate the absolute rates of diffusion-controlled enzyme reactions based on the atomic-level molecular dynamics simulations. All solvent molecules are included explicitly and the effects of the structural flexibility of enzyme, especially those of side chain motions near the active site, are included in the present calculation. In addition, the actual mobility of the substrate molecule is taken into account, which may change as the molecule approaches the active site of enzyme from the bulk solution. The absolute value of the rate constant for the wild type SOD reaction obtained from MD simulation is shown to be in good agreement with the experimental value. The calculated reactivity of a mutant SOD is also in agreement with the experimental result.

Key Words : Reaction rates, Molecular dynamics simulations, Superoxide dismutase

Introduction

Bimolecular reactions proceed in two steps, i.e., the diffusive encounter of reactants and the inherent reactive transition. For most reactions between enzymes and their substrates, the latter step controls the reaction rate. However, some enzymes show very high inherent reactivity and their overall reaction kinetics approach the diffusion controlled regime. Such enzymes are called by diffusion-controlled enzymes, and superoxide dismutase is in the category. Other examples, known so far, are acetylcholine esterase, catalase, carbon anhydrase, and so on.[1]

Brownian dynamics (BD) simulations have been widely used to calculate the rates of the diffusion-influenced enzyme reactions. McCammon and his coworkers proposed a BD method for calculating the steady-state rate constant.[2-4] In their BD method, the enzyme is fixed at the origin, and a substrate molecule starts its trajectory from a spherical surface at a distance b from the origin. Then the probability of the reactive capture of the substrate by the enzyme is calculated from the BD trajectories. This capture probability, together with an analytic expression for the rate of approach of the substrate molecule from bulk to the aforementioned spherical surface, gives the desired reaction rate constant. Since the pioneering work of McCammon and his coworkers, many authors have investigated the diffusion-influenced enzyme kinetics by using the BD simulation methods.[5-17] In particular, the BD simulation program UHBD provided by the McCammon's group has been widely used.[18]

In the present work, we will reconsider the diffusion-influenced kinetics of superoxide dismutase by using the molecular dynamics (MD) simulation method. A rigorous theoretical background for the MD method was provided recently in Ref. 19. The method is a generalization of the BD method proposed earlier by Lee and his coworkers.[20-23] In our method, the rate coefficient $k_f(t)$ is related to the *returning probability* $P_{RET}(t)$, which is the probability that a pair of reactant molecules located in the reaction zone at $t = 0$ will be found again in the reaction zone at a later time t under the condition that the reaction is absent. This quantity can be evaluated from the MD trajectories in a straightforward way. Our method has a great advantage over the simulation method of Northrup, Allison, and McCammon (NAM). As mentioned above, in the NAM method one starts the BD trajectories of the substrate molecule from a spherical surface, $r = b$. The distance should be large so that the reactive flux from the bulk to the spherical surface must be isotropic. Hence one needs an enormous number of trajectories to get the statistically reliable value for reactive capture probability, when the active site of the enzyme is screened by its side chains. For this reason, in the NAM method the enzyme structure is usually fixed with the "gate" to the active site at least partially open. In contrast, in our method the trajectories are started in the reaction zone, so that about the same number of trajectories is required to obtain the statistically reliable estimate for $P_{RET}(t)$ even when the active site of the enzyme is buried under its surface. Another advantage of our method is that only one set of MD simulations in the absence of reaction is required to calculate the diffusion-influenced reaction rates for varying values of the intrinsic reactivity of enzyme.

†This paper is to commemorate Professor Kook Joe Shin's honourable retirement.

It is expected that the mobility of the substrate molecule changes as it approaches the active site of enzyme, because of the variation in the solvation structure and also due to hydrodynamic interaction. In the BD methods, one may include the hydrodynamic interaction effects in an approximate manner, but the effects of varying solvation structure cannot be counted. On the other hand, in the present MD method we include the explicit solvent molecules and the flexibility of the enzyme structure is also counted appropriately. Hence the hydrodynamic interaction effect and the non-Markovian dynamic effect arising from the slow motions of enzyme side chains are all counted at the molecular level.

As an application of our MD method, we will investigate the kinetics of Cu/Zn superoxide dismutase (SOD), which catalyzes the conversion of the toxic superoxide anion radical, O_2^- to oxygen or hydrogen peroxide ($2O_2^- + 2H^+ \rightarrow H_2O_2 + O_2$).[24] The experimentally measured value of the bimolecular rate coefficient is 2×10^{-9} $M^{-1}s^{-1}$ for human SOD.[25,26] SOD is a homodimeric protein. Each subunit contains one copper and one zinc atoms. The Cu atom is coordinated to four histidines, forming a distorted square planar geometry. One of these histidines, His63, formally exhibits a negative charge and acts as a bridge between the Cu and Zn atoms. While the Zn atom serves to stabilize the active site structure, Cu plays an essential role in the enzymatic catalysis.[27]

The kinetics of SOD has been extensively studied by Sines *et al*.,[28] Getzoff *et al*.,[29,30] and Sergi *et al*.[31] by using the BD simulation methods. Shen *et al*.[32] and Luty *et al.* [33] obtained improved results by adding MD simulation data nearby the active site to the previously obtained BD simulation data. However, such hybridization of BD and MD methods has an inherent problem in relating the data obtained from MD simulation region to those obtained from BD simulation region. Because of the high efficiency of our MD method and the improved computing power, an investigation of the enzyme kinetics based on full atomistic MD simulations is now possible. The present work represents one of such attempts.

Theoretical Background

In Ref. 19 we formulated a general theory of the diffusion-influenced kinetics of irreversible bimolecular reactions occurring in the low concentration limit. Starting from the classical Liouville equation for the reactants and explicit solvent molecules, we derived a formally exact expression for the bimolecular reaction rate coefficient that is given by

$$s\hat{k}_f(s) = \frac{k_{eq}}{1+\hat{\Omega}(s)}. \tag{1}$$

This is an completely general rate expression; the structures of reactant molecules and solvent molecules may be arbitrarily complicated. Also, the sink functions may include all the atomistic details of the reactive events.

In Eq. (1) $\hat{k}_f(s)$ denotes the Laplace transform for the bimolecular rate coefficient, and k_{eq} is the "equilibrium" rate constant that is realized if the reactant distribution remains in equilibrium throughout the reaction process. The full expression for $\hat{\Omega}(s)$ is rather complicated, and will not be reproduced here. However, when the reaction zone, which is a subregion of the phase space in which the bimolecular reaction takes place, is so small that local equilibration in the reaction zone occurs rapidly compared to the overall reaction time scale, $\Omega(t)$ can be approximated as

$$\Omega(t) \cong N_1(t) \equiv \frac{\int d\Lambda_1 S_{AB}(\Lambda_1) \int d\Lambda_0 S_{AB}(\Lambda_0) \mathcal{G}^{(2)}(\Lambda_1,t|\Lambda_0,0) g(\Lambda_0)}{\int d\Lambda_0 S_{AB}(\Lambda_0) g(\Lambda_0)}. \tag{2}$$

Here, $S_{AB}(\Lambda)$ is the reaction sink function, which describes the decay rate of the reactant molecules at a set of relative phase-space coordinates Λ of two reacting molecules A and B. The reaction zone mentioned above is the subregion in the Λ space where $S_{AB}(\Lambda)$ has nonzero values. $g(\Lambda)$ denotes the equilibrium pair correlation function defined in the Λ space. The key dynamic quantity, $\mathcal{G}^{(2)}(\Lambda_1,t|\Lambda_0,0)d\Lambda_1$ represents the conditional probability, *averaged over all possible pairs of reactants*, that the relative coordinates of an A-B pair are within $d\Lambda_1$ at Λ_1 *in the absence of reaction*, given that they were at Λ_0 at $t = 0$. $\mathcal{G}^{(2)}(\Lambda_1,t|\Lambda_0,0)$ includes all the intricate effects of explicit solvent dynamics as well as the dynamics of nonreactive coordinates of reactant molecules. Therefore, the rate expression in Eq. (1) will enable us to evaluate the effects of non-Markovianity arising from the reaction-transport coupling and the slow relaxations of nonreactive coordinates, including inertial dynamic effects, hydrodynamic effects, and so on.

The physical meaning of $N_1(t)$ defined in Eq. (2) is most clear when the inherent reaction rate is uniform within the reaction zone [that is, if $S_{AB}(\Lambda)$ equals to a constant rate constant k_R in the reaction zone and vanishes otherwise]. Then, $k_R^{-1}N_1(t)$ is the probability that A-B pairs which were distributed in equilibrium within the reaction zone at $t = 0$ will be found in the reaction zone at time t, in a hypothetical system in which encounters in the reaction zone do not lead to reaction so that the reactants are not destroyed. When $S_{AB}(\Lambda)$ is not constant in the reaction zone, $k_R^{-1}N_1(t)$ represents a *returning probability in the absence of reaction* that is weighted appropriately by the nonuniform reaction rate.

In calculating the bimolecular rate coefficient for the SOD reaction, we will simply assume that Λ involves spatial coordinates only, and that $S_{AB}(\Lambda)$ has a constant value k_R in the reaction zone. Then Eq. (1), together with the approximation in Eq. (2), reduces to the following form,

$$s\hat{k}_f(s) = \frac{k_R V_{rx}}{1+k_R \hat{P}_{RET}(s)}. \tag{3}$$

Here, $V_{rx}[=k_R^{-1}\int d\Lambda S_{AB}(\Lambda)g(\Lambda)]$ roughly represents the volume of the reaction zone. $\hat{P}_{RET}(s)$ is the Laplace transform of the returning probability $P_{RET}(t)$, which is the probability that a pair of reactant molecules located in the reaction zone at

$t = 0$ will be found again in the reaction zone at a later time t under the condition that the reaction is absent. Hence, one can calculate the rate coefficient $k_f(t)$ as follows:

(1) Start the MD trajectories for a pair of reactant molecules from a reaction zone;

(2) Propagate the trajectories by using an appropriate move algorithm;

(3) Terminate the trajectories when the time length exceeds some cutoff time T;

(4) From the record of N trajectories of time length T, calculate $P_{RET}(t)$ as $P_{RET}(t) =$ (number of trajectories found in the reaction zone at time t)/N;

(5) Calculate V_{rx} by using an appropriate Monte Carlo method;

(6) Calculate $\hat{P}_{RET}(s)$ by numerical Laplace transformation;

(7) Calculate $k_f(t)$ by numerical inverse Laplace transformation.

The steady state rate constant is given by

$$k_f(\infty) = \frac{k_R V_{rx}}{1 + k_R \hat{P}_{RET}(0)} . \quad (4)$$

If the intrinsic rate k_R is extremely large, Eq. (4) reduces to

$$k_f(\infty) \cong k_D = V_{rx} / \int_0^\infty dt\, P_{RET}(t) . \quad (5)$$

In the case of SOD reaction, the reaction zone may be defined by the position vector $\mathbf{r}$ of the superoxide anion radical, O_2^-. One can then calculate V_{rx} as follows.

$$V_{rx} = k_R^{-1} \int d\mathbf{r}\, S(\mathbf{r}) g(\mathbf{r}) = \int_{rx} d\mathbf{r} e^{-\beta u(\mathbf{r})}$$

Here, $\int_{rx} d\mathbf{r}$ represents the integral over the reaction zone, which may be approximated by dividing the reaction zone into small, equally sized cells of volume v_{cell}:

$$V_{rx} \cong v_{cell} \sum_i \exp[-\beta \langle u(\mathbf{r}) \rangle_i]$$

$$= v_{cell} \exp[-\beta \langle u(\mathbf{r}) \rangle_{mfv}] \sum_i \frac{(\text{residence time in } i\text{th cell})}{\left(\begin{array}{c}\text{residence time in the most}\\ \text{frequently visited cell}\end{array}\right)}$$

$$= v_{cell} \exp[-\beta \langle u(\mathbf{r}) \rangle_{mfv}] \times \frac{\left(\begin{array}{c}\text{total residence time in the}\\ \text{reaction zone}\end{array}\right)}{\left(\begin{array}{c}\text{residence time in the most}\\ \text{frequently visited cell}\end{array}\right)} . \quad (6)$$

$\langle u(\mathbf{r}) \rangle_i$ is the potential of mean force at the center of the ith cell, and $\langle u(\mathbf{r}) \rangle_{mfv}$ is that for the most frequently visited cell.

Simulation Details

Reaction Systems. The three dimensional Cartesian coordinates for human SOD, which is a mutant G37R (PDB code 1AZV),[34] was taken from the Protein Data Bank and restored to wild type. The G37 residue is located at an opposite side of the enzyme from the active site, so that it will not affect the reaction dynamics much. SOD has a dimeric structure with two reaction sites. Since the distance between the two active sites is large and there is no evidence for an allosteric effect, to reduce the simulation system size, we just took chain A of the dimer, and added hydrogens in accord with the pH 7 condition. The net charge of the monomer is –2.[26]

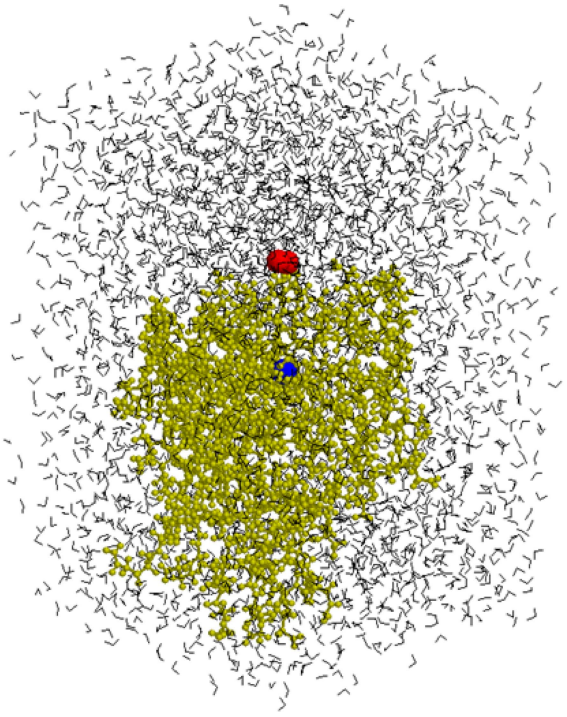

Figure 1. The simulation box contains an SOD monomer, diatomic superoxide anion radical O_2^-, and 4316 water molecules. The active site Cu atom and O_2^- are represented by blue and red van der Waals spheres, respectively, while the other atoms of SOD are represented by smaller yellow spheres.

We have calculated the partial charges of the Cu and Zn

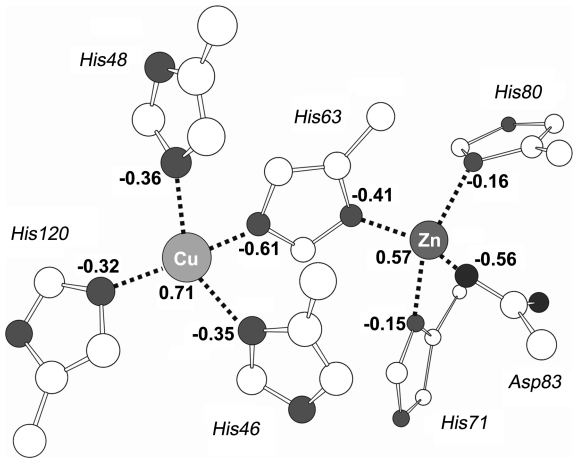

Figure 2. The optimized structure of active site residues that bind the metal ions. The numbers on Cu and Zn, nitrogen atoms of the histidine residues, and the oxygen atom of the aspartic acid residue are the recalculated partial charges by *ab initio* calculation. Geometry optimization was performed at the B3LYP/6-31G* level, and the atomic partial charges were obtained at the RHF/6-31G* level of calculation.

atoms at the active site and the nitrogen atoms of the histidine residues and the oxygen atom of the aspartic acid residue that bind the metal atoms from *ab initio* calculation at the RHF/6-31G* level, after performing the geometry optimization calculation at the B3LYP/6-31G* level. The results are depicted in Figure 2. Each oxygen of the superoxide anion radical O_2^- has a partial charge of −0.5 and a diameter of 1.7 Å. The bond strength of O_2^- was taken to be 600 kcal mol^{-1} Å^{-2}.

MD simulations were carried out with CHARMM 27b3.[35] We used the all atom models with CHARMM22 force field. The hydrogen-containing bonds were constrained by SHAKE. The SOD structure was flexible except some residues that are located at the opposite side of the enzyme from the active site. They are residues 1 to 37, 91 to 101, 116 to 120, and 145 to 155, forming mainly β-sheets. We fixed these residues to avoid the unfolding of the monomeric SOD structure and also to save the computing time. Because they are located off the active site, constraining their structures will not much affect the reaction dynamics.

In addition to SOD and O_2^-, the system contained 4,316 TIP3P water molecules in a 54 × 54 × 54 Å^3 cubic box under periodic boundary conditions. For the wild type SOD, we repeated the simulations in a larger cubic box of size 80 × 80 × 80 Å^3 to check the system size dependence. We used the Verlet/Langevin integrator for the NVT ensemble.

Calculation of the Returning Probability. At the start of each MD trajectory, the superoxide anion radical O_2^- was put into a predefined reaction zone located in the vicinity of the Cu atom. Then, during equilibration we impose a harmonic constraint on the substrate to prevent it from leaving the reaction zone. The starting structure was energy minimized by the steepest descent method for 100 steps and then by the adopted basis Newton-Raphson method for 1000 steps. The system was heated to 300 K, and equilibrated at 300 K for 5 ns with 1.5 fs time step. After this equilibration run, we saved the reaction system coordinates at every 200 ps until 1,000 different equilibrated coordinates were sampled. These equilibrated coordinates were used as the initial system configurations for generating 1,000 MD trajectories.

In the production run, we reduced the time step size to 1 fs. For each trajectory, we picked up one of the initial system coordinates, and freed O_2^- from the harmonic constraint. To stabilize the system after this little change, we equilibrated the system again for 2 ps with randomization of the velocities. In order to prevent O_2^- from getting too close to the Cu atom and being trapped there, we applied harmonic constraints to water molecules located within 5.5 Å from the Cu atom so that they block O_2^- not to intrude inside. Also, to save the computing time, only those water molecules located within 4 Å distance from SOD surface and those within 13 Å from the center of O_2^- were allowed to move. The other water molecules were fixed, although they may influence the whole reaction dynamics *via* the force fields. The "spotlighted" region of 13 Å radius around O_2^- was updated every 4 ps as O_2^- moves; it is just like the spotlight following the player on the stage.

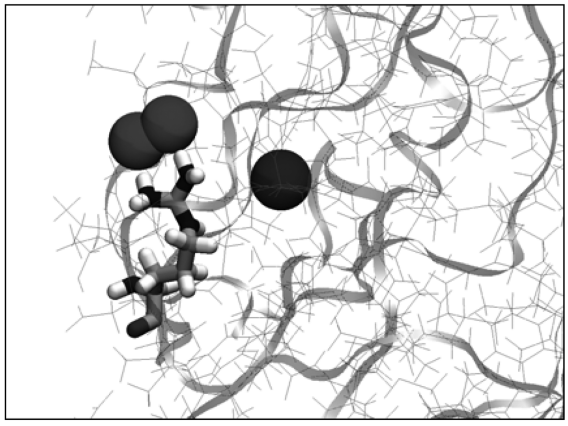

Figure 3. Two hydrogen atoms of the positively charged Arg143 are holding the oxygen atoms of O_2^- when the distance between the Cu atom and O_2^- is about 7 Å.

We recorded the distance between the active site Cu atom and O_2^- every 100 fs. The trajectory was terminated when the time length of the trajectory reached 3 ns or when the Cu-O_2^- distance became larger than 26 Å, considering that the returning probability gets negligible once O_2^- escapes to that distance. After collecting the data for 1,000 trajectories the returning probability was calculated as prescribed above.

Calculation of V_{rx}. Figure 3 shows a snapshot of the active site region of SOD obtained from an MD trajectory. It shows that the residue Arg143 is holding O_2^- when the distance between the Cu atom and O_2^- is about 7 Å. Indeed, it is believed that the SOD reaction proceeds very rapidly once an intermediate $Cu^{2+} - O_2^- -$ Arg143 is formed.[36] Indeed, it is known that the reactivities of all Arg143 mutants decrease to a great extent. Hence, we may define the reaction zone as the narrow region in the vicinity of Arg143. We thus defined the reaction zone as the region where the distance r between the active site Cu atom and O_2^- is about 7 Å. More specifically, its radial extension was defined to be $\Delta r = 1$ Å with its center varied from 7.5 Å to 8.5 Å. As shown in Figure 1, the active site of SOD is slightly buried under its surface. Hence the lateral extension of the reaction zone fluctuates as the side chains of SOD moves.

To calculate V_{rx} by using Eq. (6), we divided the reaction zone into cells of 1 Å^3 volume as schematically depicted in

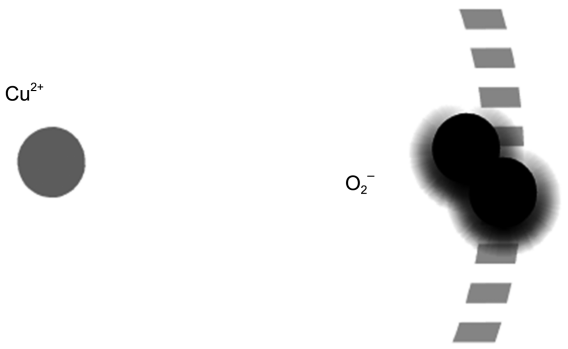

Figure 4. A schematic illustration of the division of the reaction zone into cells.

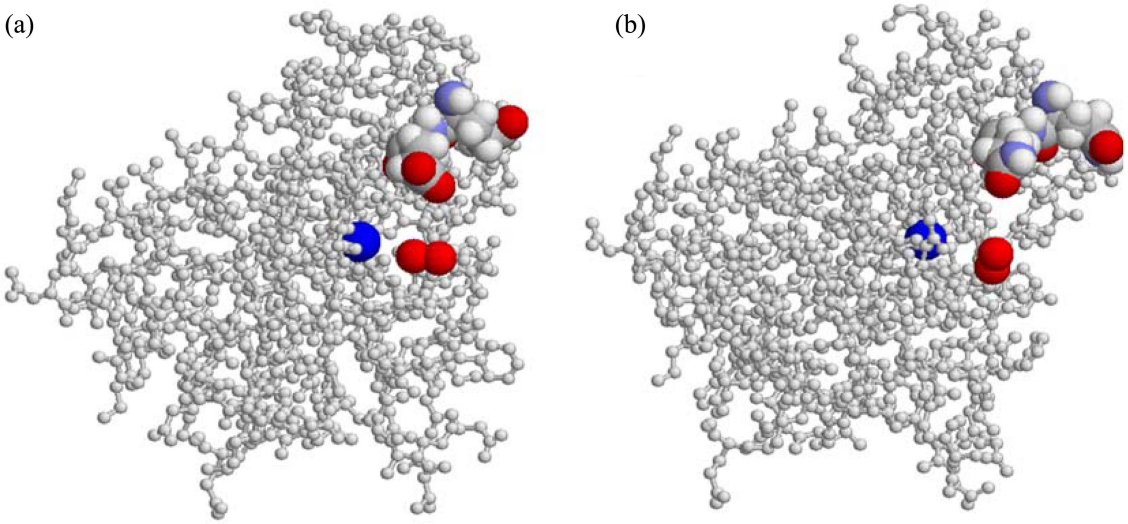

Figure 5. Structural difference between (a) the wild type SOD and (b) the mutant under consideration. Two glutamic acid residues, Glu132 and Glu133, in the wild type SOD are mutated to glutamine residues.

Figure 4. From a 10 ns trajectory in which the radial motion of O_2^- was constrained to remain within the reaction zone, we were able to obtain statistically smooth relative visit counts among the cells.

To evaluate $\langle u(\mathbf{r})\rangle_{mfv}$ defined in Eq. (6), we calculated the potential of mean force (PMF), $u(r)$, by integrating the mean repulsive force (MRF) along the radial path from $r = \infty$ to the center of the most frequently visited cell:

$$u(r) = \int_r^\infty dr\, f_{MRF}(r) \cong \int_r^{r_\infty} dr\, f_{MRF}(r) + \frac{z_{SOD} z_{SO} e^2}{\varepsilon r_\infty}. \qquad (7)$$

We have assumed that the PMF value at a large separation (denoted as r_∞) is simply given by the electrostatic potential energy, since the contributions to $u(r_\infty)$ from other molecular interactions between O_2^- and solvent molecules must be the same as those to $u(r=\infty)$. We set $r_\infty = 500$ Å, $z_{SOD} = -2$, $z_{O_2^-} = -1$, and $\varepsilon = 78$.

The MRF is a mean interacting force between O_2^- and SOD under the influence of the surrounding solvent molecules. We calculated the MRF along the radial direction from point-by-point MD simulations when r is less than 22 Å. The radial path was taken to be the straight line piercing the most frequently visited cells. To locate the center of O_2^- at a fixed distance r but to allow its rotation, we introduced a dummy atom at the center of O_2^- and fixed its position. In the MD simulations for calculating $f_{MRF}(r)$ a rectangular simulation box of the size 46 × 46 × 60 Å^3 containing 3,143 water molecules was used with SOD laid to one side of the box. We set the cutoff distance for the force field of water molecules to a quite large value of 20 Å to include the contributions from enough number of water molecules lying in the region between SOD and O_2^-. In addition, in calculating the repulsive force onto O_2^-, we included all the interacting forces from SOD atoms and water molecules located within 18 Å distance from O_2^- as well as those water molecules within 5 Å solvation shell around SOD. The repulsive forces onto O_2^- were recorded at every 5 fs from the 1 ns trajectory.

To calculate $f_{MRF}(r)$ at the larger distances from 21 Å to 500 Å, Langevin dynamics (LD) simulations were performed. In LD, the dielectric constant was set to 78, and the friction coefficient was set to 61 ps^{-1}.

Results and Discussion

Returning Probability. We have generated 1,000 trajectories for each of the wild type SOD and the mutant in Figure 5. From the MD trajectories, we calculated the returning probability $P_{RET}(t)$ as prescribed in the paragraph following Eq. (3). To calculate the diffusion-controlled rate constant k_D from Eq. (5), we need to integrate $P_{RET}(t)$ over t from 0 to infinity. Since $P_{RET}(t)$ was calculated by $t = 3$ ns, we have to make a tail correction, based on the fact that $P_{RET}(t)$ decays asymptotically as $t^{-3/2}$. The technical details of this tail correction procedure were given in a previous work,[23] and will not be reproduced here. The values of $\hat{P}_{RET}(0) = \int_0^\infty dt\, P_{RET}(t)$ obtained for the native SOD and the mutant are listed in Table 1.

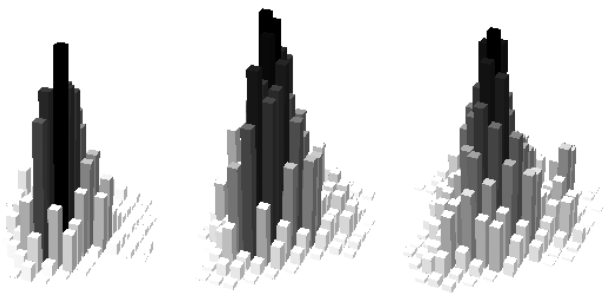

Figure 6. Visiting count distributions over the cells of reaction zone in the case of wild type SOD. From left to right, the center of reaction zone varies as $r = 7.5$ Å (reaction zone 1), 8.0 Å (reaction zone 2), and 8.5 Å (reaction zone 3), but its width is fixed ($\Delta r = 1$ Å). The volume of each cell is 1 Å^3. We see that the lateral dimension of the reaction zone increases from reaction zone 1 to 3.

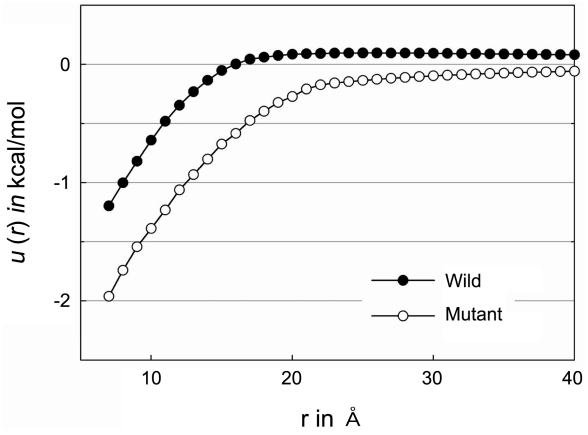

Figure 7. Potential of mean force as a function of the distance between the Cu atom of SOD and O_2^-.

The Reaction Zone Configuration Intergral, V_{rx}. V_{rx} was calculated by using Eq. (6). Figure 6 displays the bar charts for the relative residence times in the cells of 1 Å^3 volume into which the reaction zone is divided. We only display the results for the native SOD reaction. To check the possible dependence of the calculated rate constant value on the definition of the reaction zone, we obtained the results for three different definitions of the reaction zone; (i) reaction zone 1 with 7.0 Å < r < 8.0 Å, (ii) reaction zone 2 with 7.5 Å < r < 8.5 Å, and (iii) reaction zone 3 with 8.0 Å < r < 9.0 Å. As expected, Figure 6 shows that the lateral dimension of the reaction zone increases from reaction zone 1 to 3.

Figure 7 displays the variation of the potential of mean force (PMF), $u(r)$, as calculated from Eq. (7) by integrating the mean repulsive force (MRF) obtained from simulations. MRF was calculated along the radial path at 1 Å interval from 7 to 40 Å and the interval was increased gradually for r lager than 40 Å.

As shown in Figure 5, the mutant SOD has almost the same structure as the wild type SOD. The only difference between the glutamic acid residues (Glu) and the glutamine residues (Gln) is that –COOH group in Glu is replaced by –$CONH_2$ in Gln. However, at physiological pH Glu is in the negatively charged deprotonated carboxylate form, while Gln is in neutral form. Hence the net charge of the wild type and the mutant SODs are –2 and 0, respectively. There is a net repulsive interaction between the negatively charged wild type SOD and O_2^- at long distance, but in the vicinity of the active site O_2^- feels an attractive force due to the anisotropic charge distribution over the enzyme.[30] Figure 7 displays this net attractive interaction near the active site in a quantitative manner. The interaction between the neutral mutant SOD and O_2^- is attractive at all separations. The values of V_{rx} calculated from Eqs. (6) and (7) are listed in Table 1.

The Diffusion-Controlled Rate Constant, k_D. The value of k_D was calculated from Eq. (5). Note that we have calculated the rate constant for a monomeric unit of SOD. As mentioned already, the distance between the two active sites of SOD is large and there is no evidence for an allosteric effect. Hence we may assume that the actual rate constant for SOD is two times of the k_D value we obtained. The rate constant values so obtained for the wild type and the mutant SODs are listed in Table 1, together with the experimentally measured rates.[30,37]

Table 1. The diffusion-controlled rate constant of the wild type SOD and its (Glu132→Gln, Glu133→Gln) mutant. The experimental values of the rate constant are those obtained at 20 mM ionic strength and at physiological PH. The k_D values listed in parenthesis for the wild type SOD are those obtained from MD simulations with the larger simulation box of size 80 × 80 × 80 Å^3

		$\hat{P}_{RET}(0)$ in ps^{-1}	V_{rx} in Å^3	k_D in 10^9 M^{-1}s^{-1}
Wild type	Reaction zone 1	50.6	99	2.4 (1.5)
	Reaction zone 2	58.7	120	2.5 (1.8)
	Reaction zone 3	62.9	130	2.5 (1.9)
	Experiment			2.3
Mutant	Reaction zone 1	56.5	249	5.3
	Reaction zone 2	60.5	279	5.6
	Reaction zone 3	69.0	319	5.6
	Experiment			7.2

First, we note that the calculated rate constant values are rather insensitive to the location of the reaction zone, unless it is placed unphysically at the outside of the active site pocket. On the other hand, the calculated results depends considerably on the size of the simulation box. However, we believe that the size of the larger simulation box (80 × 80 × 80 Å^3) is large enough that the results would not change much even if one further increases the box size.

The experimental values for the rate constant decreases as the ionic strength of the solution increases,[38,39] but are rather insensitive to pH as long as pH < 8. Our simulated reaction system corresponds to the zero ionic strength condition. The experimental data quoted in Table 1 are the values at 20 mM ionic strength. There is no experimental data at zero ionic strength, but the rate constant values extrapolated to the zero ionic strength are in the range of 3-4 × 10^9 M^{-1}s^{-1} for wild type SOD and 8-9 × 10^9 M^{-1}s^{-1} for the mutant SOD.[30,38,39] Considering the complexity of the reaction system, we see that our calculated values of k_D are in good agreement with the experimental values.

Conclusion

We carried out MD simulations to calculate the diffusion-controlled steady-state rate constant of SOD reactions based on the recently proposed general theory of diffusion-influenced reactions.[19] The key quantities calculated from the MD trajectories are the returning probability $P_{RET}(t)$ and the reaction zone configuration integral V_{rx}. We obtained the results that are in fair agreement with the experimental results for both wild type and mutant enzymes.

Considering the complexity of the reaction system that includes all the solvent molecules and the flexible enzyme

molecules, we believe that this is a remarkable achievement. Unlike the BD simulation methods, the present MD method is a kind of a "first-principle" method, in that the only inputs are the CHARMM potential parameters and the effective charges of the active site atoms calculated from an *ab initio* calculation. With the rapid advance of the computing power of multi-core workstations, the present MD method can be applied to calculate the rate constant for more complicated diffusion-controlled enzymes.

Acknowledgments. This work was supported by the grants from National Research Foundation (NRF), funded by the Korean Government (Grant Nos. 2009-0074693 and 2010-0001631).

References

1. Berg, J. M.; Tymoczko, J. L.; Stryer, L. *Biochemistry*, 5th ed.; Freeman: New York, 2002.
2. Northrup, S. H.; Allison, S. A.; McCammon, J. A. *J. Chem. Phys*. **1984**, *80*, 1517.
3. McCammon, J. A.; Northrup, S. H.; Allison, S. A. *J. Phys. Chem.* **1986**, *90*, 3901.
4. Luty, B. A.; McCammon, J. A.; Zhou, H.-X. *J. Chem. Phys.* **1992**, *97*, 5682.
5. Antosiewicz, J.; Briggs, J. M.; McCammon, J. A. *Eur. Biophys. J.* **1996**, *24*, 137.
6. Antosiewicz, J.; McCammon, J. A. *Biophys. J*. **1995**, *69*, 57.
7. Song, Y.; Zhang, Y.; Shen, T.; Bajaj, C. L.; McCammon, J. A.; Baker, N. A. *Biophys. J.* **2004**, *86*, 2017.
8. Chung, S. H.; Allen, T. W.; Kuyucak, S. *Biophys. J*. **2002**, *83*, 263.
9. Northrup, S. H.; Luton, J. A.; Boles, J. O.; Reynolds, J. C. *J. Comput. Aided Mol. Des*. **1988**, *1*, 291.
10. Tan, R. C.; Truong, T. N.; McCammon, J. A.; Sussman, J. L. *Biochemistry* **1993**, *32*, 401.
11. Tara, S.; Elcock, A. H.; Kirchhoff, P. D.; Briggs, J. M.; Radic, Z.; Taylor, P.; McCammon, J. A. *Biopolymers* **1998**, *46*, 465.
12. Wade, R. C.; Davis, M. E.; Luty, B. A.; Madura, J. D.; McCammon, J. A. *Biophys. J*. **1993**, *64*, 9.
13. Zhou, H. X. *Biophys. J*. **1993**, *64*, 1711.
14. Zhou, H. X.; Briggs, J. M.; Tara, S.; McCammon, J. A. *Biopolymers* **1998**, *45*, 355.
15. Zhou, H. X.; Szabo, A. *Biophys. J*. **1996**, *71*, 2440.
16. Huber, G. A.; Kim, S. *Biophys. J*. **1996**, *70*, 97.
17. Zou, G.; Skeel, R. D.; Subramaniam, S. *Biophys. J*. **2000**, *79*, 638.
18. Davis, M. E.; Madura, J. D.; Luty, B. A.; McCammon, J. A. *Computer Phys. Comm*. **1991**, *62*, 187.
19. Kim, J.-H.; Lee, S. *J. Chem. Phys*. **2009**, *131*, 014503.
20. (a) Lee, S.; Karplus, M. *J. Chem. Phys*. **1987**, *86*, 1883. (b) Lee, S.; Karplus, M. *J. Chem. Phys*. **1987**, *86*, 1904. (c) Lee, S.; Karplus, M. *J. Chem. Phys*. **1992**, *96*, 1663.
21. Yang, S.; Kim, J.; Lee, S. *J. Chem. Phys*. **1999**, *111*, 10119.
22. Yang, S.; Han, H.; Lee, S. *J. Phys. Chem. B* **2001**, *105*, 6017.
23. Lee, J.; Yang, S.; Kim, J.; Lee, S. *J. Chem. Phys*. **2004**, *120*, 7564.
24. McCord, J. M.; Fridovich, I. *J. Biol. Chem*. **1969**, *244*, 6049.
25. Rotilio, G.; Bray. R. C.; Fielden, E. M. *Biochim. Biophys. Acta*. **1972**, *268*, 605.
26. Klug, D.; Rabani, J.; Fridovich, I. *J. Biol. Chem.* **1972**, *247*, 4839.
27. Tainer, J. A.; Getzoff, E. D.; Richardson, J. S.; Richardson, D. C. *Nature* **1983**, *306*, 284.
28. Sines, J. J.; Allison, S. A.; McCammon, J. A. *Biochemistry* **1990**, *29*, 9403.
29. Getzoff, E. D.; Tainer, J. A.; Weiner, P. K.; Kollman, P. A.; Richardson, J. S.; Richardson, D. C. *Nature* **1983**, *306*, 287.
30. Getzoff, E. D.; Cabelli, D. E.; Fisher, C. L.; Parge, H. E.; Viezzoli, M. S.; Banci, L.; Hallewell, R. A. *Nature* **1992**, *358*, 347.
31. Sergi, A.; Mauro, F.; Polticelli, F.; O'Neill, P.; Desideri, A. *J. Phys. Chem.* **1994**, *98*, 10554.
32. Shen J.; McCammon, J. A. *Chem. Phys*. **1991**, *158*, 191.
33. Luty, B. A.; Amrani, S. E.; McCammon, J. A. *J. Am. Chem. Soc.* **1993**, *115*, 11874.
34. Hart, P. J.; Liu, H.; Pellegrini, M.; Nersissian, A. M.; Gralla, E. B.; Valentine, J. S.; Eisenberg, D. *Protein Sci*. **1998**, *7*, 545.
35. Brooks, B. R.; Bruccoleri, R. E.; Olafson, B. D.; States, D. J.; Swaminathan, S.; Karplus, M. *J. Comput. Chem*. **1983**, *4*, 187.
36. Osman, R.; Basch, H. *J. Am. Chem. Soc.* **1984**, *106*, 5710.
37. Fisher, C. L.; Cabelli, D. E.; Hallewell, R. A.; Beroza, P.; Lo, T. P.; Getzoff, E. D.; Tainer, J. A. *Proteins* **1997**, *29*, 103.
38. Cudd, A.; Fridovich, I. *J. Biol. Chem*. **1982**, *257*, 11443.
39. Argese, E.; Viglino, P.; Rotilio, G.; Scarpa, M.; Rigo, A. *Biochemistry* **1987**, *26*, 3224.